JOURNAL OF PROPULSION AND POWER
Vol. 10, No. 5, Sept.–Oct. 1994

Investigation of Supersonic Jet Plumes Using an Improved Two-Equation Turbulence Model

B. Lakshmanan*
Old Dominion University, Norfolk, Virginia 23529
and
Khaled S. Abdol-Hamid†
Analytical Services and Materials, Inc., Hampton, Virginia 23661

Supersonic jet plumes were studied using a two-equation turbulence model employing corrections for compressible dissipation and pressure-dilatation. A space-marching procedure based on an upwind numerical scheme was used to solve the governing equations and turbulence transport equations. The computed results indicate that two-equation models employing corrections for compressible dissipation and pressure-dilatation yield improved agreement with the experimental data. In addition, the numerical study demonstrates that the computed results are sensitive to the effect of grid refinement and insensitive to the type of velocity profiles used at the inflow boundary for the cases considered in the present study.

Nomenclature

D = initial diameter of the jet
k = turbulent kinetic energy
M = Mach number
P = static pressure
P_k = production of the turbulent kinetic energy
R = gas constant
r = radial coordinate
T = static temperature
t = time
u = velocity component in the axial direction
x = axial coordinate
α = model constants for compressibility and pressure-dilatation corrections in Eqs. (7) and (8)
γ = ratio of specific heats
ε = dissipation of turbulent kinetic energy
μ = dynamic molecular viscosity
ρ = density
σ = spreading rate of the jet, $\sigma = (dy_{1/2U}/dx)$
ω = vorticity

Subscripts
c = centerline
j = jet
l = laminar
t = turbulent
∞ = freestream

Introduction

THE recent resurgent interest in a High Speed Civil Transport (HSCT) and the National AeroSpace Plane (NASP) clearly demonstrates the need for advanced propulsion systems for supersonic velocities and beyond. Because of the complexity of the problem, numerous research programs have been initiated. One aspect of this research has been directed towards detailed understanding of the complex flowfield associated with the engine over a wide range of operating conditions. Computational fluid dynamics (CFD) in conjunction with recent advances in turbulence modeling is being used extensively for detailed investigation of the propulsion related flowfield. Currently, there is a renewed interest in the flow properties of compressible mixing layer and jet plumes since it is central to many advanced propulsion systems. In addition, the classical fluid physics represented by this problem makes it ideally suited for basic numerical studies.

An effort is currently underway to investigate the aerodynamics of jet plumes, where the shear layer interacts strongly with the shock structure in much of the jet plume flowfield. It is widely accepted that the computational economy of the two-equation turbulence models offers the best compromise for computing complex turbulent shear flows. However, some deficiencies remain in these models that restrict their use in complex situations. In particular, the local density extensions of standard incompressible turbulence models were found to be inadequate in duplicating the experimentally observed reduction in growth rate of the mixing layer with increasing convective Mach number. Various modifications[1–3] have been suggested, but none appear to model the physics of the flow adequately when parameters beyond mean growth rate are considered. Recently, Sarkar et al.[4] and Sarkar[5] recognized the importance of including compressible dissipation and pressure-dilatation effects in the two-equation turbulence models when computing high-speed flows. Simple corrections were proposed for compressible dissipation and pressure-dilatation that can be easily included in the existing two-equation turbulence models. In addition, Dash[6] included an axisymmetric correction in the turbulence transport equations when solving jet problems to account for vortex stretching. The standard two-equation model is recovered when the model constants for these corrections are assumed to be zero.

During the past decade, considerable progress has been made in the area of CFD. Most of the research activities have been centered around developing efficient numerical algorithms for the solution of parabolized and full Navier-Stokes equations. Chief among these are upwind schemes because they are robust and efficient with good convergence properties. Complex three-dimensional laminar and turbulent flows

Received April 27, 1992; presented as Paper 92-2604 at the AIAA 10th Applied Aerodynamics Conference, Palo Alto, CA, June 22–24, 1992; revision received Feb. 17, 1994; accepted for publication Feb. 23, 1994.

*Research Associate, Department of Mechanical Engineering and Mechanics; currently Research Assistant Professor, NASA Langley Research Center, Propulsion Aerodynamics Branch, M/S 409, Hampton, VA 23681. Member AIAA.

†Senior Research Scientist, CFD Section; currently NASA Langley Research Center, Hampton, VA 23681. Member AIAA.

over realistic aerodynamic configurations have been routinely simulated using these schemes. Despite the popularity of upwind schemes, their extension to solving stiff equations are limited in literature, especially within the framework of space-marching procedures.

Since the streamwise gradients are small in mixing layer/jet plume problems, space-marching procedures are attractive alternatives to time-marching procedures. Lakshmanan and Abdol-Hamid[7] had studied the high-speed shear layer using an implicit upwind space-marching code containing the compressibility corrected two-equation turbulence model. The space marching was found to be highly efficient: two-orders of magnitude reduction of the residual was achieved in less than 15 iterations in each marching plane using a CFL number as high as 15.

The primary objective of the present work is to incorporate axisymmetric correction, compressible dissipation, and pressure-dilatation terms in the two-equation turbulence model. The resulting model is then utilized to compute high-speed compressible jet plumes. Another objective of the work is to investigate the effect of inflow profiles and grid refinement on the computed flowfield.

Theoretical Formulation

Governing Equations

The theoretical formulation of the problem starts with the Favre-averaged form of the equations representing conservation of mass, momentum, energy, and turbulence quantities. The overbar is used to denote a conventional Reynolds average, whereas the tilde is used to denote the Favre-average. For the sake of brevity, only the k and ε equations are given here. Extensive details of the governing equations can be found in Ref. 8:

k-Equation

$$\frac{\partial}{\partial t}(\bar{\rho}\tilde{k}) + \frac{\partial}{\partial x_k}\left(\bar{\rho}\tilde{k}\tilde{u}_k - \mu_k\frac{\partial \tilde{k}}{\partial x_k}\right) = P_k - \bar{\rho}(\tilde{\varepsilon}_s + \tilde{\varepsilon}_c) + \overline{p''d''} \tag{1}$$

ε-Equation

$$\frac{\partial}{\partial t}(\bar{\rho}\tilde{\varepsilon}_s) + \frac{\partial}{\partial x_k}\left(\bar{\rho}\tilde{\varepsilon}_s\tilde{u}_k - \mu_\varepsilon\frac{\partial \tilde{\varepsilon}_s}{\partial x_k}\right) = (C_1P_k + \bar{\rho}\tilde{\varepsilon}_s\{-C_2 + C_3\chi\})\frac{\tilde{\varepsilon}_s}{\tilde{k}} \tag{2}$$

where $P_k = -\bar{\rho}u_i'u_j'(\partial\tilde{u}_i/\partial x_j)$ is the production of the turbulent kinetic energy. Here, $-\bar{\rho}u_i'u_j'$ is the Reynolds stress, and μ_k and μ_ε are defined as follows:

$$-\bar{\rho}u_i'u_j' = \mu_t\left(\frac{\partial\tilde{u}_i}{\partial x_j} + \frac{\partial\tilde{u}_j}{\partial x_i}\right) - \frac{2}{3}\delta_{ij}\left(\mu_t\frac{\partial\tilde{u}_k}{\partial x_k} + \bar{\rho}\tilde{k}\right) \tag{3}$$

$$\mu_k = \mu_l + (\mu_t/\sigma_k) \tag{4a}$$

$$\mu_\varepsilon = \mu_l + (\mu_t/\sigma_\varepsilon) \tag{4b}$$

$$\mu_t = C_\mu\bar{\rho}(\tilde{k}^2/\tilde{\varepsilon}) \tag{5}$$

In Eq. (4), μ_l and μ_t represent the laminar and turbulent coefficients of viscosity, respectively. The model constants used in the analysis are $C_\mu = 0.09$, $C_1 = 1.44$, $C_2 = 1.92$, $C_3 = 0.79$, $\sigma_k = 1.0$, and $\sigma_\varepsilon = 1.3$. In Eq. (1), ε_c and $\overline{p''d''}$ represent the contributions due to compressible dissipation and pressure-dilatation, and χ is the axisymmetric correction. The compressible and pressure-dilatation effects are included using recently developed models[4,5] based on direct numerical simulation of isotropic turbulence. A simplified form of the axisymmetric correction used by Dash[6] is used in the present analysis. This additional term represents the contribution due to vortex stretching in axisymmetric flows. The details of the corrections are given as follows:

Axisymmetric correction

$$\chi = \frac{1}{4}\left(\frac{\tilde{k}}{\tilde{\varepsilon}_s}\right)^3\left(\frac{\partial\tilde{u}}{\partial r} - \frac{\partial\tilde{v}}{\partial x}\right)^2\frac{\tilde{v}}{r} \tag{6}$$

Model for compressible dissipation

$$\tilde{\varepsilon}_c = \alpha_1 M_t^2\tilde{\varepsilon}_s \tag{7}$$

Model for pressure-dilatation

$$\overline{p''d''} = -\alpha_2\bar{\rho}P_kM_t^2 + \alpha_3\bar{\rho}\tilde{\varepsilon}_sM_t^2 \tag{8}$$

where $M_t = \sqrt{2\tilde{k}/\gamma RT}$ is the turbulent Mach number, and ε_s is the solenoidal dissipation. Based on direct numerical simulation, Sarkar[5] recommends $\alpha_1 = 0.5$, $\alpha_2 = 0.4$, and $\alpha_3 = 0.2$.

Boundary Conditions

The boundary conditions to be imposed are problem-dependent. In the case of jet plume calculations, four types of boundaries are encountered. These include inflow, outflow, symmetry, and outer boundaries. Riemann invariants were used along the outer boundary corresponding to the external freestream. Symmetry boundary conditions were applied along the axis of symmetry. At the inflow boundary, three different initial velocity profiles were studied to investigate their effect on the computed flowfield. These include an experimentally measured velocity profile,[9] a hyperbolic tangent profile, and a top-hat profile. Since the solutions were obtained by a marching procedure, the downstream boundary conditions were left unspecified.

For the turbulence transport equations either zeroth-order extrapolation or freestream values are used for k and ε along the outer boundaries. If the flow is outgoing along the outer boundary, zeroth-order extrapolation is used. If there is flow entrainment, then freestream values are used along the outer boundaries. At the inflow laminar solutions were computed for the first three planes, and thereafter the k-ε turbulence model is turned on. The inflow profile for k takes the same shape as the vorticity profile except it is multiplied by a specified value of maximum turbulence intensity (Fig. 1). Once the k profile is known, the ε profile is obtained using production equals dissipation hypothesis. Since the k-ε equations were solved by a marching procedure, the downstream boundary conditions were left unspecified.

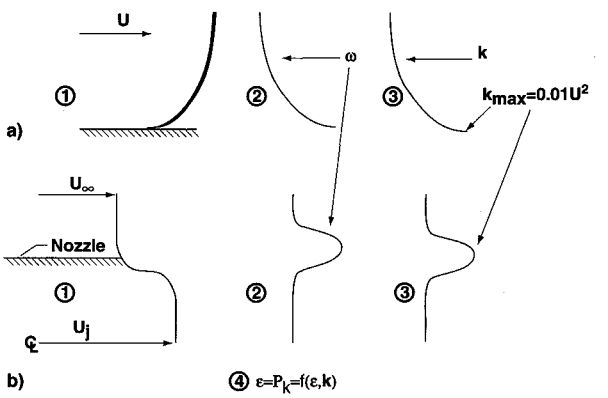

Fig. 1 Inflow boundary condition for k-ε turbulence model: a) flat plate and b) jet flow.

Method of Solution

The governing equations for the mean flow and turbulence quantities were integrated using an implicit upwind numerical procedure employing the approximate-factorization technique. The numerical code used in this study has been designed to accommodate multiblock/multizone grid configurations. Two numerical algorithms are available in the code: 1) van Leer flux-vector splitting and 2) Roe's flux difference splitting. In addition, the code has options for three different algebraic turbulence models and a two-equation Jones-Launder turbulence model.

Depending on the complexity of the problem, this code has the capability to compute the flowfield using either the space-marching or the time-marching procedures. It should be noted that when using a space-marching procedure for supersonic/subsonic mixing problems, the upstream influence from all the points downstream is neglected. However, not all the streamwise derivatives are dropped. In particular, the streamwise pressure gradient is fully retained in the supersonic regions of the flow. In the subsonic region of the flow, the streamwise pressure gradient term is dropped. This approach is valid as long as the pressure gradient is negligible. Extensive details of the numerical scheme, turbulence models, and the capabilities of the code can be found in Ref. 10.

Results and Discussion

Supersonic jet plumes (Figs. 2 and 3) exhausting into a nominally stationary external stream were computed using an improved form of the two-equation turbulence model. In all the cases, the initial jet radius was equal to 1.28 cm. Because of the axisymmetric nature of the problem, only a sector of the jet was computed. The outer boundary of the computational domain in the radial direction was located at eight radius from the jet axis.

A compact algebraic grid generation program[11] was used for generating the mesh. The computations employed 401 equally spaced points in the axial direction. A grid refinement study was carried out in the radial direction employing 81, 101, and 121 points. Grid-independent results were obtained for computations employing 121 points. Approximately 61 points were located in the initial jet radius with a typical grid spacing of 0.036 cm at the axis and 0.005 cm along the lip line. It should be noted that of the 61 points used in the jet, 41 points were placed between 0–1.18 cm, and the remaining 21 points were placed in the narrow region between 1.18–1.28 cm. Using this grid resolution it was possible to interpolate the velocity profiles available from the experimental measurements.[9] The remaining 61 points were distributed between the lip line and the outer boundary using a cubic distribution of grid cell sizes.

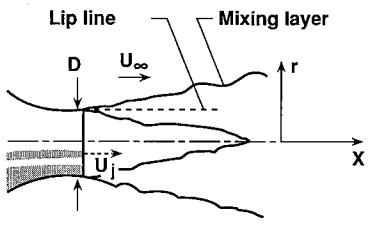

Fig. 2 Schematic of a fully expanded supersonic jet plume.

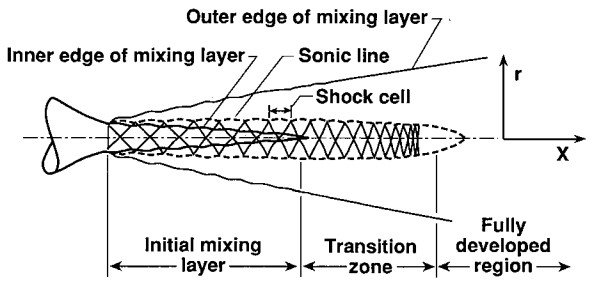

Fig. 3 Schematic of an underexpanded supersonic jet plume.

The average computational time for each case is approximately 140 CPU seconds on the Cray 2 computer. Approximately 10–15 iterations were needed in each plane to achieve two orders-of-magnitude reduction of the residual using a CFL number as high as 15. The computed results did not differ significantly when the calculations were allowed to achieve three orders-of-magnitude reduction of the residual.

For cases of an under or overexpanded jet flow, the calculation was carried up to 20 jet diameters in the streamwise direction. For fully expanded jet plumes the computation was carried up to 40 jet diameters in the axial direction. The freestream conditions for all the cases were

$$M_\infty = 0.05, \quad P_\infty = 101{,}325 \text{ N/m}^2, \quad T_\infty = 293 \text{ K}$$

Case 1: Fully Expanded Supersonic Jet

A fully expanded supersonic jet exhausting into the assumed freestream condition was computed. For this case, the jet operating conditions were

$$M_j = 2.2, \quad P_j/P_\infty = 1.0, \quad T_j/T_\infty = 1.0$$

The computations were compared with the experimental measurements of Eggers.[9] Figure 4 shows the effect of axisymmetric correction on the centerline velocity. These results are obtained using the turbulence model employing correc-

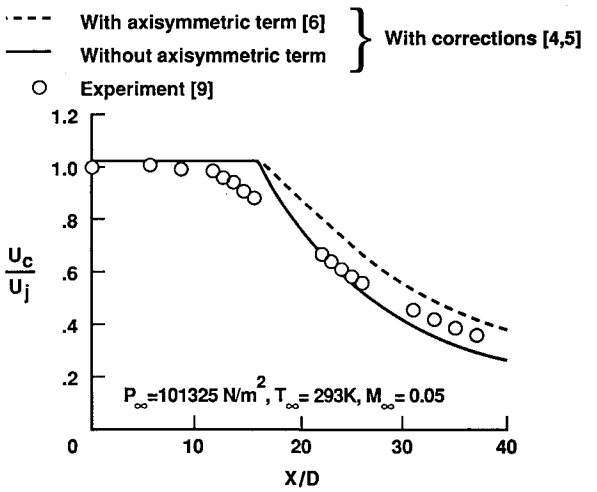

Fig. 4 Effect of axisymmetric correction on the centerline velocity for a fully expanded supersonic jet plume.

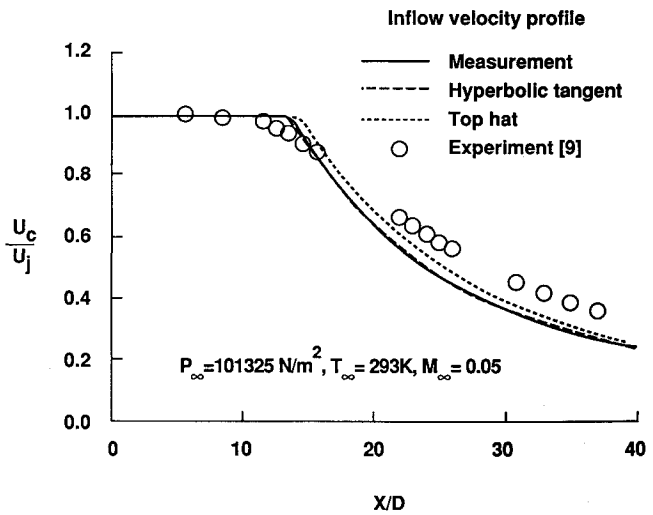

Fig. 5 Effect of inflow profiles on the centerline velocity for a fully expanded supersonic jet plume.

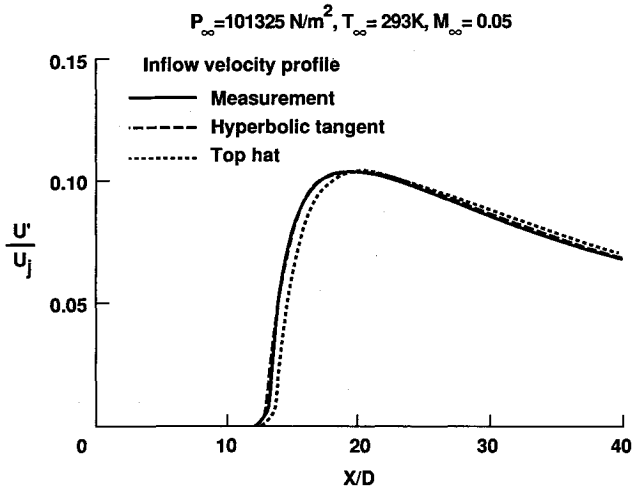

Fig. 6 Effect of inflow profiles on the centerline turbulence intensity for a fully expanded supersonic jet plume.

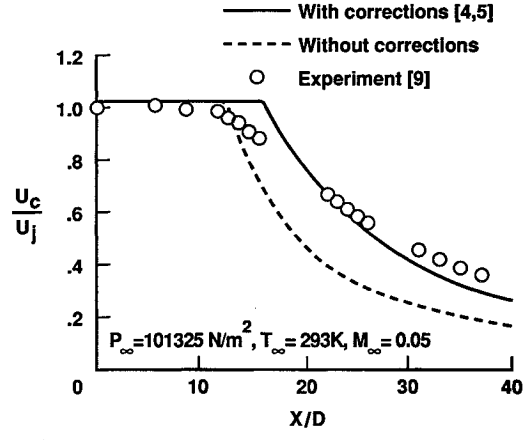

Fig. 7 Effect of compressibility and pressure-dilatation corrections on the centerline velocity for a fully expanded supersonic jet plume.

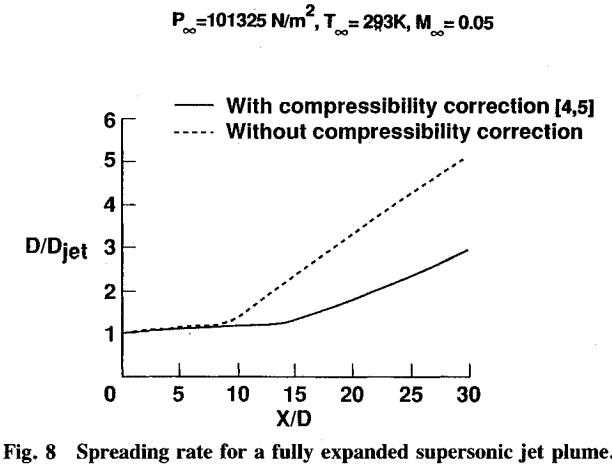

Fig. 8 Spreading rate for a fully expanded supersonic jet plume.

tions for compressible dissipation and pressure-dilatation effects. It is clear that by using the axisymmetric correction, slightly slower decay rate for the jet is observed. On the other hand, without the axisymmetric correction better agreement with the data for the velocity decay is obtained. In addition, numerical difficulties were experienced with the axisymmetric correction term when computing shock containing jet plumes. As a result, the axisymmetric correction term is neglected in subsequent computations. Figures 5 and 6 show the effect of inflow profiles on the centerline velocity and turbulence intensity. These results show that the centerline values are insensitive to the type of profiles used at the inflow boundary.

Figure 7 presents the effect of compressibility and pressure-dilatation corrections on the computed centerline velocity. It is clear that the standard turbulence model provides a faster velocity decay, whereas the turbulence model with corrections yields a velocity decay that is in better agreement with the experimental data. The core length (distance required for mixing layer to reach the jet centerline) predicted by the standard turbulence model was about $11D$, whereas the estimated length using the model with corrections was about $16D$. Experimental results indicate a core length of about $10D$. Figure 8 shows the jet spreading rate with and without compressibility correction. It is clear that the model without correction predicts a higher growth rate as compared to the compressibility corrected model.

Figure 9 presents a comparison of the computed axial velocity profile at $X/D = 13.5$ and experimental data. The turbulence model with corrections predicts a velocity profile that is in good agreement with the experimental data, although the standard turbulence model significantly underpredicts the measured velocity profile in the center of the jet and overpredicts it near the edges.

Figure 10 shows the normalized spreading rate for a fully developed flow (σ_0 being the incompressible spreading rate equal to 0.1) as a function of the jet Mach number. It is clear that computations without any compressibility correction to the models ($\alpha = 0.0$) show only a mild decrease in spreading rate with an increase in Mach number. However, inclusion of the compressibility correction to the models ($\alpha = 1.0$) lead to a sharp reduction in growth rate in the high Mach number regime. These results are in general agreement with Langley experimental data for compressible mixing layer.

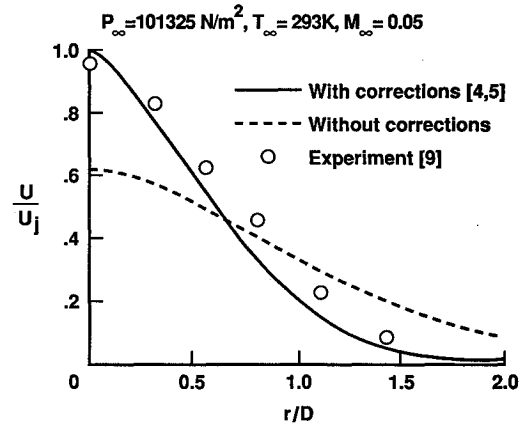

Fig. 9 Comparison of axial velocity profile at $X/D = 13.5$ with experimental data for a fully expanded supersonic jet plume.

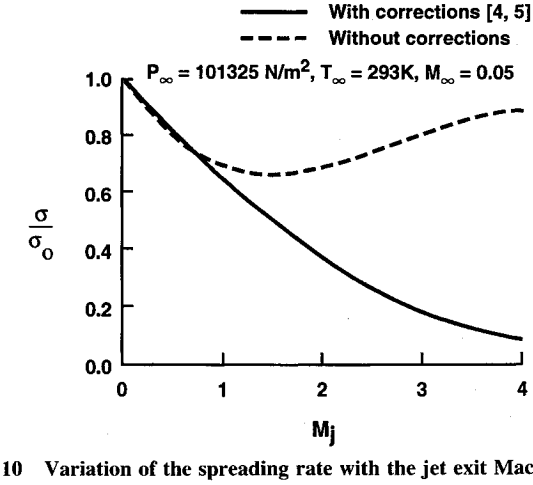

Fig. 10 Variation of the spreading rate with the jet exit Mach number.

Case 2: Underexpanded Supersonic Jet

An underexpanded supersonic jet was computed for an identical freestream condition as in the previous case: In this case, the jet operating conditions were

$$M_j = 2.0, \qquad P_j/P_\infty = 1.4, \qquad T_j/T_\infty = 1.0$$

Figure 11 shows the computed results using the turbulence model and comparison with the experimental data.[12] The computed results are shown for the first 20 jet diameters in which 8 shock cells occur. The computations slightly underpredict the peak pressure in the first four cells of the jet. However, the shock cell spacing is predicted well. Figure 12 shows the effect of turbulence model with and without corrections on the computed pressure distribution along the jet axis. The results obtained using the standard turbulence model and the turbulence model with corrections are in good agreement for the first three cells. Beyond these three cells, the standard turbulence model predicts a faster decay of the remaining shock cell structure. Figure 11 also shows the effect of grid refinement on the computed centerline pressure distribution. It is clear that results obtained using refined mesh are in better agreement with the experimental data than the coarse mesh results in which the jet shock structure is displaced slightly towards the right.

The computed rms values of the streamwise turbulence intensity shown in Fig. 13 along the jet lipline indicate a large improvement in the results when compressibility and pressure-dilatation corrections are included. Here, the experimental data are available only up to 10 jet diameters. In general, the agreement of computed results using the standard turbulence model with the experimental data was not good. The measurements and the computed results indicate that the turbulence intensity amplifies to reach peak values at the end

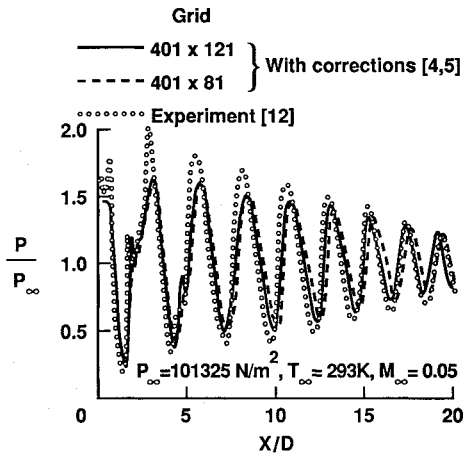

Fig. 11 Comparison of centerline pressure distribution for an underexpanded supersonic jet plume.

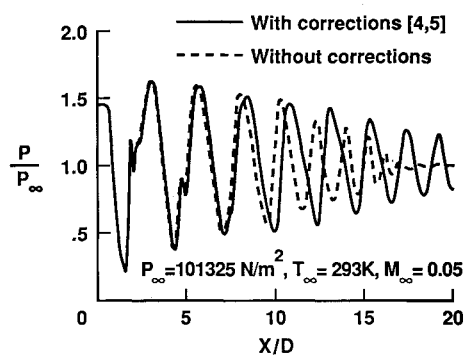

Fig. 12 Effect of compressibility and pressure-dilatation corrections on the computed centerline pressure distribution for an underexpanded supersonic jet plume.

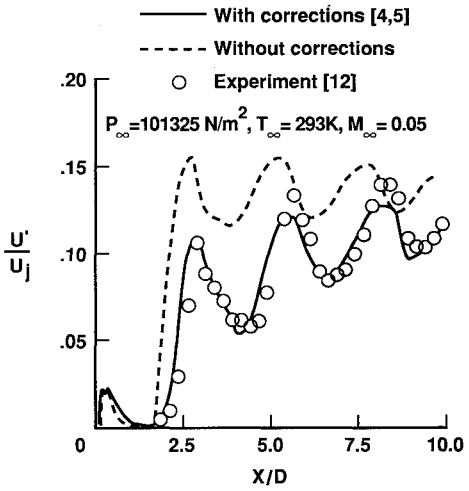

Fig. 13 Effect of compressibility and pressure-dilatation corrections on the lip line turbulence intensity for an underexpanded supersonic jet plume.

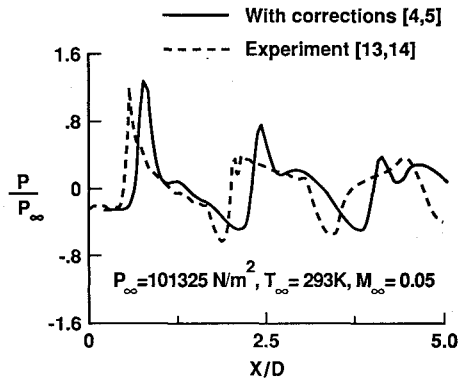

Fig. 14 Comparison of centerline pressure distribution for an overexpanded supersonic jet plume.

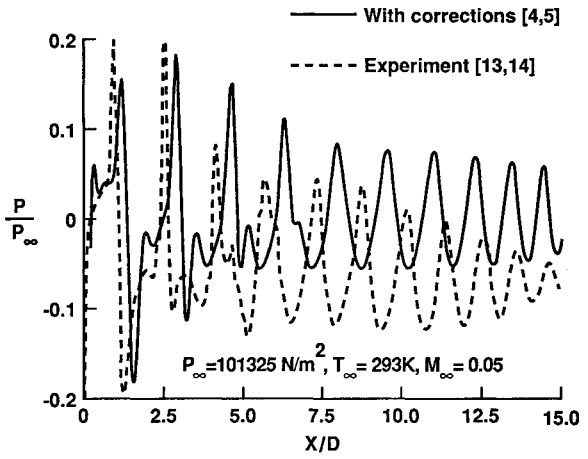

Fig. 15 Comparison of pressure distribution along the radial line $r/D = 0.375$ for an overexpanded supersonic jet plume.

of compression zones and minimum values at the end of expansion zones.

Case 3: Overexpanded Supersonic Jet

An overexpanded supersonic jet was computed for identical conditions given in the previous case except for the difference in pressure ratio at the nozzle exit. In this case, the jet operating conditions were

$$M_j = 2.0, \qquad P_j/P_\infty = 0.7, \qquad T_j/T_\infty = 1.0$$

The computed results for the pressure distribution along the jet axis and a radial line $r/D = 0.375$ are shown in Figs. 14 and 15, respectively. The centerline pressure distribution shown in Fig. 14 represents the axial extent of available data for this case. The numerical solution predicts the irregular looking pressure data[13,14] reasonably well. The comparison of the computed pressure distribution and the experimental data along the outer radial line is very good for the first three shock cells. The location and magnitude of the peak pressure were predicted well in the computations. In the downstream region, significant differences were observed in the shock wave length between the computed results and the experimental values, suggesting that measured jet plume has a faster jet spreading rate.

Concluding Remarks

Compressible high-speed jet plumes were studied using a two-equation turbulence model. It was observed that for supersonic/subsonic mixing problems, converged results could be obtained efficiently by using the space-marching procedure. In addition, corrections for compressible dissipation and pressure-dilatation for the two-equation turbulence model were tested for high-speed jet plumes. For supersonic jets, the turbulence model with corrections had significantly improved the agreement between computed results and experimental data. Moreover, the numerical study demonstrated that the computed jet decay rate was sensitive to grid resolution and insensitive to the type of profiles used at the inflow boundary.

Acknowledgments

This work was supported by the Propulsion Aerodynamics Branch at NASA Langley Research Center, Hampton, Virginia. The authors would like to acknowledge S. P. Pao of NASA Langley Research Center for providing an algebraic grid generation program for generating the computational mesh used in this study.

References

[1]Oh, Y. H., "Analysis of Two-Dimensional Free Turbulent Mixing," AIAA Paper 74-594, June 1974.

[2]Dash, S., Weilerstein, G., and Vaglio-Laurin, R., "Compressibility Effects in Free Turbulent Shear Flows," Advanced Technology Labs., ATL TR 220, Westburty, NY, 1975.

[3]Vandromme, D., "Contribution a la Modelization et la Prediction d'Ecoulements Turbulents a Masse Volumique Variable," Sc.D. Thesis, Univ. des Sciences et Techniques de Lille, France, Sept. 1983.

[4]Sarkar, S., Erlebacher, G., Hussaini, M. Y., and Kreiss, H. O., "The Analysis and Modeling of Dilatational Terms in Compressible Turbulence," NASA Langley Research Center, Inst. for Computer Applications in Science and Engineering Rept. 89-79, Hampton, VA, Dec. 1989.

[5]Sarkar, S., "Modeling the Pressure-Dilatation Correlation," NASA Langley Research Center, Inst. for Computer Applications in Science and Engineering Rept. 91-42, Hampton, VA, May 1991.

[6]Dash, S., "Observations on Practical Turbulence Modeling for High-Speed Jet/Plume Flowfields," AIAA Paper 91-1789, June 1991.

[7]Lakshmanan, B., and Abdol-Hamid, K. S., "Application of Space Marching Procedure for Transport Equation Turbulence Models," *Proceedings of the 4th International Symposium on Computational Fluid Dynamics* (Davis, CA), 1991.

[8]Abdol-Hamid, K. S., "Three-Dimensional Calculations for Underexpanded and Overexpanded Supersonic Jet Flows," *Proceedings of the AIAA 7th Applied Aerodynamics Conference* (Seattle, WA), AIAA, Washington, DC, 1989, pp. 289–293.

[9]Eggers, J. M., "Velocity Profiles and Eddy Viscosity Distribution Downstream of a Mach 2.2 Nozzle Exhausting into Quiescent Air," NASA TN D-3601, Sept. 1966.

[10]Abdol-Hamid, K. S., Uenishi, K., and Turner, W. M., "Three-Dimensional Upwinding Navier-Stokes Code with k-ε Model for Supersonic Flows," AIAA Paper 91-1669, June 1991.

[11]Pao, S. P., "Axisymmetric and Rectangular Grid Generation Package 'axb'," Version 1, NASA Langley Research Center, Hampton, VA, July 1992.

[12]Seiner, J. M., "The Wedge Hot-Film Anemometer in Supersonic Flow," NASA TP-2134, May 1983.

[13]Seiner, J. M., and Norum, T. D., "Aerodynamic Aspects of Shock Containing Jet Plumes," AIAA Paper 80-0965, June 1980.

[14]Seiner, J. M., and Norum, T. D., "Experiments of Shock Noise on Supersonic Jets," AIAA Paper 79-1526, July 1979.